Hysteresis effect on austenite-martensite interface in Ni-Mn-Ga single crystal

Chengguan Zhang[a], Guoshun Qin[a], Shaobin Zhang[b], Xue Chen [c], Yongjun He[a,] *

[a] *UME, ENSTA Paris, Institut Polytechnique de Paris, 91120 Palaiseau, France*

[b] *School of Mechanics, Civil Engineering and Architecture, Northwestern Polytechnical University, Xi'an, China*

[c] *Faculty of Engineering and Environment, Northumbria University, Newcastle Upon Tyne, UK*

* Corresponding Author. Email address: yongjun.he@ensta-paris.fr (Y. He)

Abstract

The experiments on Ni-Mn-Ga single crystal shape memory alloy under a heating-cooling cycle demonstrate that the automatically generated twin laminate structure of the compatible austenite-martensite interface in the forward martensitic phase transition is significantly different from that in the reverse phase transition, even though the temperature hysteresis is small (A_s-M_s around 4 ^oC). Moreover, after the cooling-induced austenite → martensite transition, the remaining twin laminate is so fine (layer width around 1 μm) that the neighbouring twin boundaries merge with each other and disappear, making the fine twin laminate evolve into a single martensite variant (i.e., spontaneous detwinning). These observations provide insights into the relation between the hysteresis (phase-transition driving forces), austenite-martensite interface, and the basic material parameters such as twin boundary energy and softening modulus during the phase transition.

Keywords: Hysteresis, austenite-martensite interface, spontaneous detwinning, martensitic phase transition, shape memory alloy.

Ni-Mn-Ga is a shape memory alloy (SMA) which is able to take a phase transition between a high-temperature phase (austenite) and a low-temperature phase (martensite) under certain thermo-magneto-mechanical conditions [1-7]. Because the martensitic phase transition belongs to the first order phase transition, the lattice microstructure has sudden change (cubic austenite to approximately tetragonal martensite in Fig. 1(a)) and the macroscopic deformation stains have sudden jumps across an austenite-martensite interface (A-M interface) [8]. In other words, from macroscopic point of view, a bar (or a plate) of single crystal SMA takes the phase transformation via the A-M interface nucleation and the propagation. To avoid large elastic energy caused by the strain jumps, certain orientations of the A-M interface and the associated meso-scale structures (laminates of martensite twins) are automatically selected/generated as predicted by the compatibility analysis [9-12].

Among many meso-scale twin structures, the two patterns in Fig. 1(b) (parallel laminate and branching laminate) are often observed and have been intensively studied with the energy-minimization principle [4, 12-16], from which a criterion of the energetic preference for the two patterns was obtained [14]:

$$\frac{\beta}{\alpha} = \begin{cases} Small \ \rightarrow \ \ Parallel\ laminate \\ Large \rightarrow Branching\ \ laminate \end{cases} \tag{1}$$

That means, if the austenite's elastic modulus (β) is much smaller than that of martensite (α), the parallel laminate would be energetically preferred; by contrast, if the ratio β/α is large, the branching laminate would appear. The material properties α and β are usually assumed to be constants (independent of temperature) for simplicity in the existing models of the twin laminates; so, their predictions imply that each SMA should choose only one of the two patterns

and it would have the same pattern during the forward and reverse phase transition (without hysteresis effect).

However, from the basic theories of phase transitions such as Landau theory for SMAs [17, 18], it is well known that the stability of the two phases (austenite and martensite) changes significantly at the phase transition. Particularly, austenite becomes unstable and changes to martensite (stable state) during cooling below M_s (martensite start temperature of phase transition); that is to say, the austenite's modulus (β) is much smaller than that of martensite (α), i.e., the ratio β/α is small. On the contrary, during heating above A_s (austenite start temperature of phase transition), martensite becomes soft (unstable) and austenite is stable (i.e., the ratio β/α becomes large). The material softening in SMAs such as Ni-Mn-Ga near phase transitions has been measured by Dynamic Mechanical Analysis [19, 20], the inelastic neutron scattering [21, 22], the thermal diffuse x-ray intensity [23, 24], the surface acoustic waves [25] and the ultrasonic techniques [26] where modulus reduction around 60% was captured. That means, austenite is very soft (near unstable) and martensite is stiff (very stable) during the cooling-induced forward phase transition (A→M) while the opposite case occurs in the heating-induced reverse transition (M→A). Combining the concept of material softening and the criterion Eq. (1), it is natural to expect that the cooling-induced A→M transition and the heating-induced M→A transition might have different twin patterns (parallel and branching laminates respectively). That is confirmed by the following experiments on a bar of Ni-Mn-Ga single crystal SMA (with A_s = 52°C, A_f = 55°C, M_s = 48°C, and M_f = 45°C from ETO) under heating-cooling cycles with the maximum and minimum operation temperatures around 100°C and 10°C respectively.

As shown in Fig. 2(a), we adopted two optical cameras to observe the bar's two surfaces so to obtain the full-field DIC strain maps (with software VIC-2D) during the heating-cooling cycle (with a heater for heating and a block of ice for cooling). It is seen in Fig. 2(b) that both

the cooling-induced transition (from austenite to the single martensite variant M_3) and the heating-induced transition (from M_3 to austenite) occur via the A-M interface propagation. Although a transitional zone near the A-M interface can be seen (for example $t_2^{cooling} \sim t_4^{cooling}$ in Fig. 2(b)), the full-field DIC strain maps have not enough resolution to distinguish the details of the twin structures. So, we adopted a microscope to replace the optical camera to observe a small region of the bar's surface on *x*-*y* plane during the cooling-heating cycle; then, the twin structure formation and evolution were clearly captured and recorded into Movie 1 and Movie 2 (in the supplementary materials) whose typical frames are given in Fig. 3.

As shown in the left column $t_1^{cooling}$ and $t_2^{cooling}$ of Fig. 3(b), the cooling-induced A-M interface is accompanied by a very fine twin parallel laminate consisting of numerous layers (bands). The layers in fact belong to the two martensite variants, M_3 and M_2, whose volume fraction ratio is approximately 2:1 (i.e., their volume percentages are 68% and 32% respectively); this twin composition is determined by the observed orientation of the A-M interface combined with the compatibility analysis [11] and the macroscopic DIC strains of the twin laminates (details in the Appendix in the supplementary materials). When the A-M interface passes through and becomes far from the observed region ($t_3^{cooling}$ and $t_4^{cooling}$ in Fig. 3(b)), the layers of the minor component (M_2) intermittently disappear and the observed region changes from the twin laminate to an almost single variant M_3 which agrees with the measured macroscopic deformation strains in the full-field DIC strain maps ($t_5^{cooling}$ in Fig. 2(b)). On the contrary, during heating as shown in the right column $t_1^{heating} \sim t_4^{heating}$ of Fig. 3(b), the A-M interface is accompanied by a branching twin laminate whose layers' width and spacing depend on the distance (*l*, measured along *x*-axis) from the A-M interface which are analysed in the following Fig. 4.

As shown in the schematic of Fig. 4(a), we can choose a representative area (the yellow dashed box) where the width (*d*) of the M_2 layer (the layer of the twin's minor component) and

the layer spacing (λ) can be defined. In analysing the microscopic observation, we choose the representative area at different distances from the A-M interface as shown in "RA_1" ~ "RA_4" of Fig. 4(a). The percentage (η) of M_2 layers in the representative areas can be calculated via ImageJ software and the results are summarized in Fig. 4(b) showing the dependence of η on the distance l. We can also count the number (N) of M_2 layers within the representative area (whose width $\Delta y \approx 0.6$ mm) and calculate the M_2 layer density $\rho = \frac{N}{\Delta y}$ (or domain spacing $\lambda = \frac{1}{\rho} = \frac{\Delta y}{N}$) as shown in Fig. 4(c). Then the width d of the M_2 layer can be determined by $d = \eta \cdot \lambda = \frac{\eta}{\rho}$ in Fig. 4(d) that demonstrates the significant difference between the two twin structures — the cooling-induced parallel laminate and the heating-induced branching patterns: the width d of the M_2 layer is small (around 1 μm) and keeps almost constant in the parallel pattern; by contrast, in the branching pattern, it is much larger (maximum near 9 μm) and changes non-monotonically with the distance l.

Nevertheless, the two patterns (parallel and branching laminates) share a common feature as shown in Fig. 4(b): they have the same volume fraction η of M_2 around 32% near the A-M interface (l < 1mm) as predicted by compatibility analysis [11]. By contrast, when l > 1mm, η decreases with increasing l (becoming far away from the A-M interface). By the comparison of the distance-dependent volume fraction η between the heating and cooling processes in Fig. 4(b), it can be seen that η drops to zero at $l \approx 4$ mm for heating branching laminate, much more drastically than cooling parallel laminate. In other words, the effective thickness of the A-M interface (the length of the whole twin laminate along the specimen's length direction or x-axis direction) in the heating process is smaller than that in cooling process. On the other hand, the density ρ of the M_2 layers of cooling is much higher than that of heating as shown in Fig. 4(c): for example, at $l \approx$ 1mm, there are more than 300 layers per mm (i.e., M_2 layer spacing $\lambda = 1/\rho$ around 3.3 μm) in cooling parallel laminate while less than 50 layers per

mm (λ larger than 20 μm) in heating laminate. In summary, except having the same volume fraction $\eta \approx 32\%$ for compatibility at the A-M interface, the two twin laminates during cooling and heating are significantly different from each other. To explain and understand such difference, more theoretical analysis combining the existing energy-minimizing models and the softening properties of the phase transition need to be developed in the future.

It is also indicated by the current study that, although the temperature hysteresis is small ($\Delta T_{hysteresis} = As - Ms = 52\ ℃ - 48\ ℃ = 4\ ℃$ for the current Ni-Mn-Ga bar), the hysteresis effect on the twin formation cannot be ignored because the forward and reverse martensitic phase transitions generate significantly different patterns of the twin laminates at the compatible A-M interface. With the energy analysis of the different twin laminates, it is possible to provide insight into the material phase-transforming behaviours. For example, the authors of [27] have proposed to link the hysteresis (or the driving force of phase transition) to the energy for generating the twins of the compatible A-M interface. On the other hand, based on the energy analysis on a twin laminate of Ni-Mn-Ga single crystal SMA (similar to our sample), the authors in [4] have estimated one of the basic material properties: surface energy density of the twin boundary $\gamma_{TB} = 5.8\ mJ/m^2$. As shown in the following with this twin boundary energy γ_{TB}, we can understand the spontaneous detwinning, which makes the parallel twin laminate evolve into a single martensite variant in the observation $t_2^{cooling} \sim t_4^{cooling}$ of Fig. 3(b) where the M_2 layers automatically disappear.

The disappearance of a layer can be seen as the merging and annihilation of the layer's two twin boundaries, whose energy reduction (driving force for the layer annihilation) is $\Delta E_{driving} = 2 \cdot \gamma_{TB}$ while the energy dissipation (resistant force) is $\Delta E_{dissipation} = \sigma_{tw} \cdot \varepsilon_{MR} \cdot d_n$ where $\sigma_{tw} = 0.2$ MPa is the twinning stress (i.e., frictional stress of the twin boundary movement, which has the same value for both Type I and Type II twin boundaries near phase transition temperature [28], $\varepsilon_{MR} = 6\%$ is the deformation strain during the martensite reorientation [29]

and d_n is the moving distance of the twin boundary, i.e. the distance between the M_2-layer's two twin boundaries along the twin-plane normal direction $[0, \frac{1}{\sqrt{2}}, \pm\frac{1}{\sqrt{2}}]$ [11]. So, $d_n = d\cdot\cos45^o \approx 1$ μm$\cdot \frac{1}{\sqrt{2}} \approx 0.7$ μm for the M_2 layer of the cooling parallel laminate in Fig. 4(d). With these values of the parameters γ_{TB}, σ_{tw}, ε_{MR}, and d_n, the driving force ($\Delta E_{driving} \approx 11.6$ mJ/m^2) is larger than the resistant force ($\Delta E_{dissipation} \approx 8.4$ mJ/m^2), implying that the annihilation of the M_2 layers can spontaneously occur to make the cooling parallel laminates evolve into a single martensite variant as in $t_2^{cooling} \sim t_4^{cooling}$ of Fig. 3(b). To the best knowledge of the authors, this is the first report in literature about the observation and discussion on the spontaneous detwinning in the fine twin laminate after the cooling A→M transition. We wonder whether such phenomenon only occurs in Ni-Mn-Ga single crystal SMA. More careful experiments on other SMAs are worthy to perform to reveal the relation among the hysteresis (the required phase-transition driving forces), austenite-martensite interface, and the basic material parameters such as twin boundary energy and softening modulus.

Graphical abstract

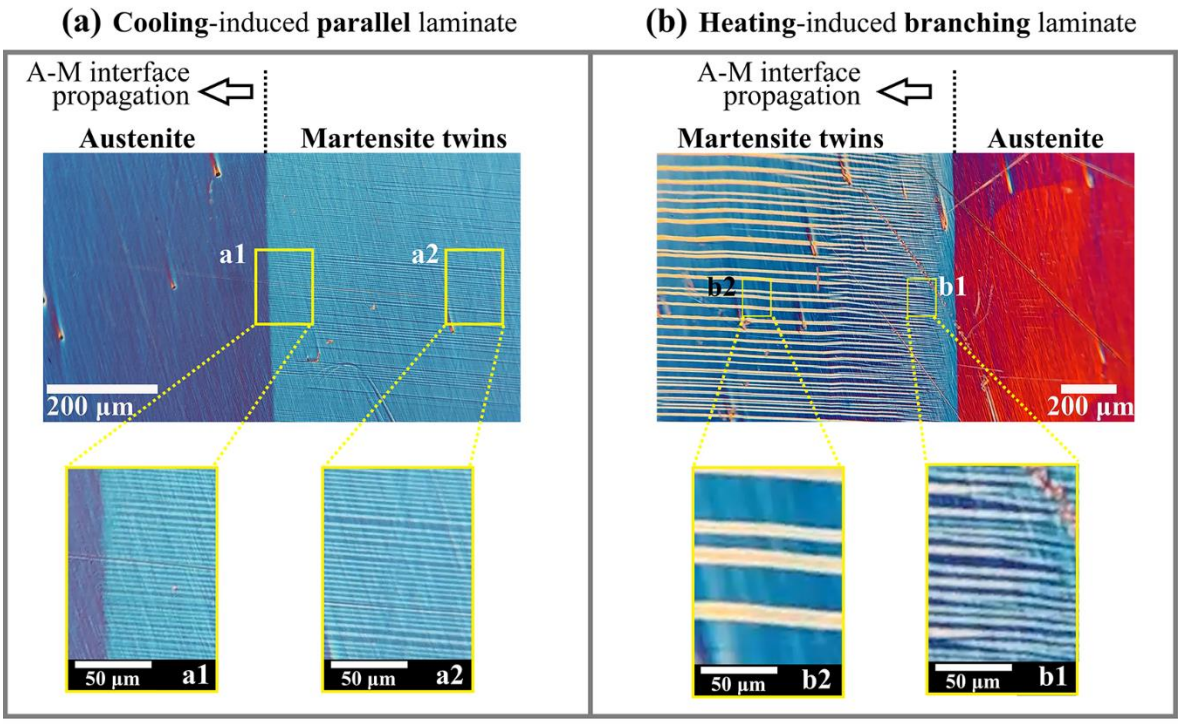

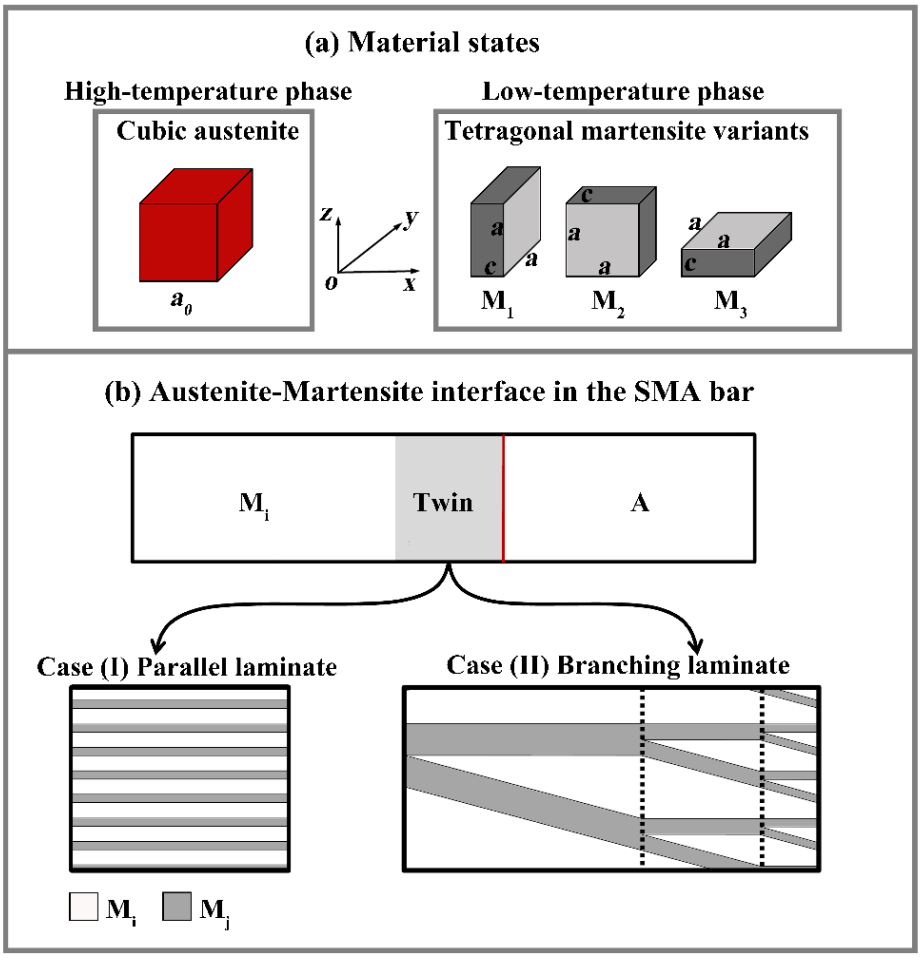

Fig. 1 (a) The material can take cubic austenite phase at high temperatures and tetragonal martensite phase at low temperatures. The three martensite variants (M_1, M_2, and M_3) have the short axis c along the *x*-, *y*-, and *z*- directions, respectively; (b) two typical twin patterns at the austenite-martensite interface: parallel laminate and branching laminate consisting of two different martensite variants M_i and M_j.

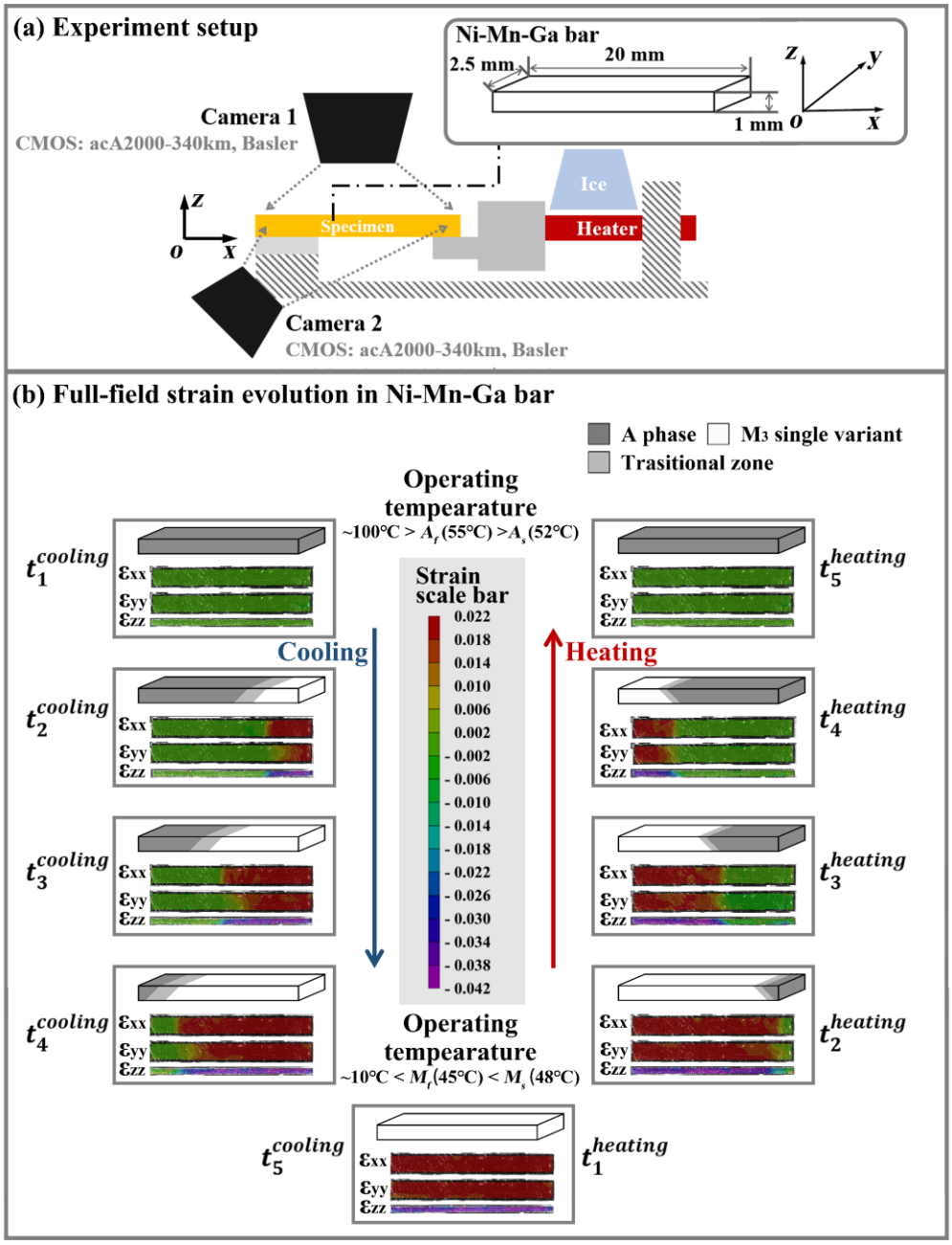

Fig. 2 (a) The experimental setup for heating-cooling cycles; (b) the schematics and DIC measurements of the strain components on the *x*-*y* plane and *x*-*z* plane. The total cooling time (heating time) is 140 s (200 s) in the current study. The symbols $t_1^{cooling}$, $t_2^{cooling}$, $t_3^{cooling}$, $t_4^{cooling}$, and $t_5^{cooling}$ correspond to the time moments 0 s, 85 s, 100 s, 115 s, and 130 s respectively during the cooling. The symbols $t_1^{heating}$, $t_2^{heating}$, $t_3^{heating}$, $t_4^{heating}$ and $t_5^{heating}$ correspond to 0 s, 60 s, 80 s, 100 s, and 200 s respectively during the heating.

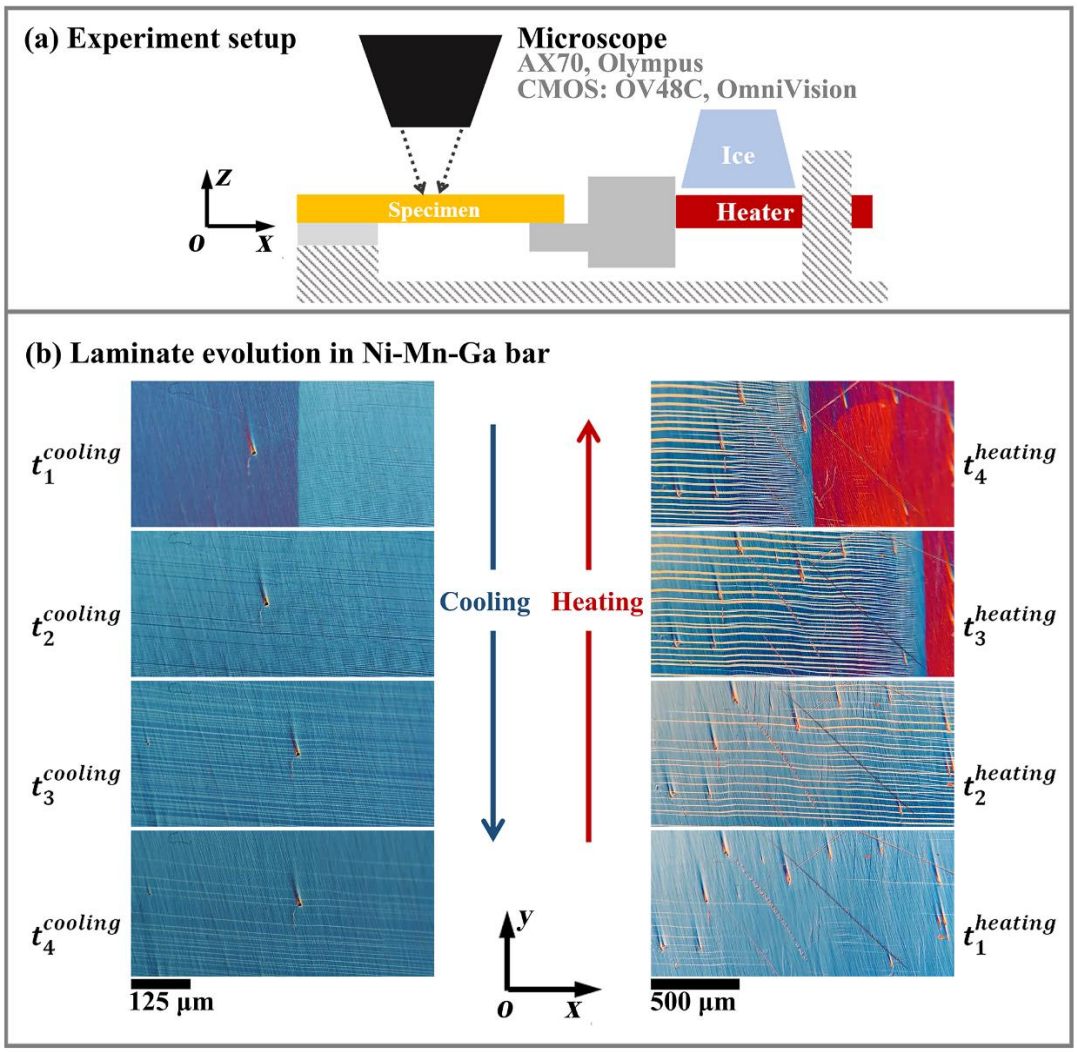

Fig. 3 The observations with a microscope on the evolution of the twin laminates of the austenite-martensite interface during cooling-heating cycles. The frames $t_1^{cooling} \sim t_4^{cooling}$ and $t_1^{heating} \sim t_4^{heating}$ are from movie 1 and movie 2 respectively in the supplementary materials. The symbols $t_1^{cooling} \sim t_4^{cooling}$ correspond to the time moments 0.8 s, 3.8 s, 11.8 s, and 28 s respectively in movie 1. The symbols $t_1^{heating} \sim t_4^{heating}$ correspond to the time moments 1.6 s, 12.6 s, 18.7 s, and 21 s respectively in movie 2.

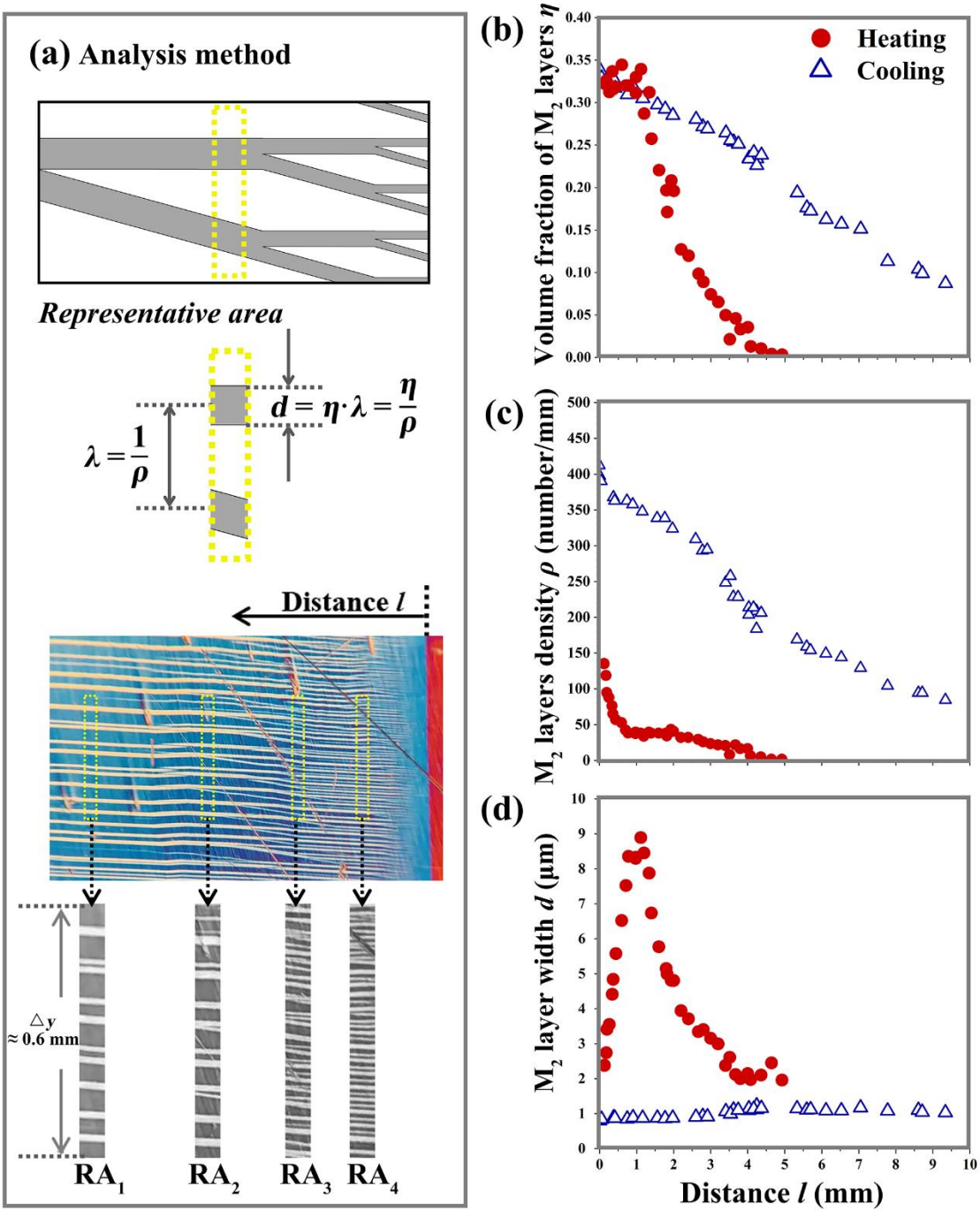

Fig. 4 (a) Analysis method to extract the features of the twin laminates, which depend on the distance l from the A-M interface: (b) volume fraction η of the twin's minor component (M_2 variant), (c) M_2 layers density ρ, and (d) M_2 layer width d.

Reference

[1] H.E. Karaca, I. Karaman, B. Basaran, D.C. Lagoudas, Y.I. Chumlyakov, H.J. Maier, Acta Mater. 55(13) (2007) 4253-4269.

[2] K. Haldar, D.C. Lagoudas, I. Karaman, J. Mech. Phys. Solids 69 (2014) 33-66.

[3] V. Pinneker, M. Gueltig, A. Sozinov, M. Kohl, Acta Mater. 64 (2014) 179-187.

[4] E. Bronstein, E. Faran, D. Shilo, Acta Mater. 164 (2019) 520-529.

[5] S. Zhang, X. Chen, Z. Moumni, Y. He, Int. J. Plasticity 108 (2018) 1-20.

[6] X. Chen, Y. He, Int. J. Plasticity 129 (2020) 102686.

[7] C. Yu, T. Chen, H. Yin, G. Kang, D. Fang, Int. J. Solids struct. 191-192 (2020) 509-528.

[8] O. Heczko, N. Lanska, O. Soderberg, K. Ullakko, J. Magn. Magn. Mater. 242-245 (2002) 1446-1449.

[9] J.M. Ball, R.D. James, Fine phase mixtures as minimizers of energy, Arch. Ration. Mech. Anal. 100 (1987)13–52.

[10] K. Bhattacharya, Microstructure of Martensite: Why it Forms and How it Gives Rise to the Shape-memory Effect, Oxford University Press, Oxford, 2003.

[11] S. Zhang, X. Chen, Z. Moumni, Y. He, Int. J. Plasticity 110 (2018) 110-122.

[12] S. Stupkiewicz, G. Maciejewski, H. Petryk, Acta Mater. 55(18) (2007) 6292-6306.

[13] G. Arlt, J. Mater. Sci. 25 (1990) 2655-2666.

[14] R.V. Kohn, S. Müller, Philos. Mag. A 66(5) (1992) 697-715.

[15] H. Seiner, P. Plucinsky, V. Dabade, B. Benešová, R.D. James, J. Mech. Phys. Solids 141 (2020).

[16] B. Horovitz, G.R. Barsch, J.A. Krumhansl, Phys. Rev. B 43(1) (1991) 1021-1033.

[17] F. Falk, Acta Metall. 28 (1980) 1773-1780.

[18] F. Falk, Le Journal de Physique Colloques 43(C4) (1982) C4-3-C4-15.

[19] C. Segui, E. Cesari, J. Pons, V.A. Chernenko, V.V. Kokorin, J. Phys. IV France 06(C8) (1996) C8-381-C8-384.

[20] V.V. Kokorin, V.A. Chernenko, E. Cesari, J. Pons, C. Segui, Journal of physics: condensed matter 8 (1996) 6457-6463.

[21] A. Zheludev, S. M. Shapiro, P. Wochner, Phys. Rev. B 54(21) (1996) 15045.

[22] U. Stuhr, P. Vorderwisch, V.V. Kokorin, P.-A. Lindgard, Phys. Rev. B 56(22) (1997) 14360-14365.

[23] G. Fritsch, V.V. Kokorin, A. Kempf, Journal of physics: condensed matter 6 (1994) L107-L110.

[24] G. Landmesser, U. Klemradt, R.L. Johnson, T.R. Finlayson, Appl. Phys. Lett. 90(2) (2007).

[25] O. Heczko, H. Seiner, P. Stoklasová, P. Sedlák, J. Sermeus, C. Glorieux, A. Backen, S. Fähler, M. Landa, Acta Mater. 145 (2018) 298-305.

[26] L. Mañosa, A. Gonzàles-Comas, E. Obrado, A. Planes, V.A. Chernenko, V.V. Kokorin, E. Cesari, Phys. Rev. B 55(17) (1997) 11068-11071.

[27] Z. Zhang, R.D. James, S. Müller, Acta Mater. 57(15) (2009) 4332-4352.

[28] L. Straka, A. Soroka, H. Seiner, H. Hänninen, A. Sozinov, Scripta Mater. 67(1) (2012) 25-28.

[29] O.Z. Pascan, Y.J. He, Z. Moumni, W.H. Zhang, Scripta Mater. 104 (2015) 71-74.